Virtual Histology (VH) for Detecting Necrotic Core (NC)

37

Giancarla Scalone, Salvatore Brugaletta, and Manel Sabaté

Contents

Abstract

The ultimate characteristics of an atherosclerosis plaque at any given time depend on the relative contribution of its components. In particular, necrolipidic core is known to be the most thrombogenic component of atheromatous plaque. Therefore, the presence of fibroatheroma with a lipid-rich necrotic core and a thin fibrous cap (TCFA) appears particularly prone to rupture and subsequent coronary artery occlusion. Coronary angiography is unable to assess the magnitude

G. Scalone • S. Brugaletta • M. Sabaté (✉)
Cardiology Department, Thorax Institute, Hospital Clinic, Institut d'Investigacions Biomediques August Pi i Sunyer (IDIBAPS), Barcelona, Spain
e-mail: gcarlascl@gmail.com; sabrugaletta@gmail.com; masabate@clinic.ub.es

V.B. Patel, V.R. Preedy (eds.), *Biomarkers in Cardiovascular Disease*, Biomarkers in Disease: Methods, Discoveries and Applications, DOI 10.1007/978-94-007-7678-4_30

and composition of atherosclerotic burden. The recent development of novel intracoronary imaging methods able to detect plaque composition, such as intravascular ultrasound virtual histology (VH-IVUS), may represent a breakthrough in acute coronary syndrome prevention. In the future, a more extensive use of multiple image technologies in a single catheter, as VHS-IVUS and optical coherence tomography or near-infrared spectroscopy, will be likely to provide a more comprehensive assessment of the coronary vasculature. These imaging technologies and their clinical/research applications are discussed in detail in this section.

Keywords
Intravascular ultrasound imaging • Virtual histology • Necrotic core

Abbreviations

ACS	Acute coronary syndrome
BVS	Bioabsorbable stent
DES	Drug eluting stent
HR	Hazard ratio
IVUS-VH	Intravascular ultrasound virtual histology
LCBI	Lipid-core burden index
LCP	Lipid core plaque
LDL	Low-density lipoprotein/cholesterol
MACE	Major acute coronary events
MI	Myocardial infarction
NCCL	Necrotic core in contact with the lumen
NIRS	Near-infrared spectroscopy
OCT	Optical coherence tomography
PAV	Percent atheroma volume
PCI	Percutaneous coronary intervention
RF	Radiofrequency
ROC	Receiver-operating characteristic curve
SA	Stable angina
TCFA	Thin cap fibroatheroma

Key Factors of Vulnerable Plaque

- Acute coronary syndromes are mostly caused by sudden coronary thrombosis due to rupture of vulnerable plaques with a large lipid core or by erosion of endothelium within fibrous plaques.
- The precursor lesion of symptomatic heart disease is characterized by a large necrotic core and an overlying fibrous cap thinner than <65 μm, and is rich in inflammatory cells with a few smooth muscle cells.
- The necrolipidic core is known as the most thrombogenic component of atheromatous plaque due to its high content in tissue factor.

- Optical coherence tomography can provide a high-resolution image (10–20 μm) of the thin fibrous cap, but it is not able to detected a large and deep lipid core because of its limited penetration (<2 mm).

Key Factors of Necrotic Core

- Necrotic core of the coronary plaque has been variously related to clinical risk factors, and also associated with cardiac adverse events.
- The detection of plaques with high risk of rupture could prevent future occurrence of acute coronary syndrome.
- Virtual histology actually represents the gold standard to study the presence of necrotic core in the atherosclerotic plaque.

Definitions

Atheroma Atheromatous plaques are formed by an intricate sequence of events, not necessarily in a linear chronological order, that involves extracellular lipid accumulation, endothelial dysfunction, leukocyte recruitment, intracellular lipid accumulation (foam cells), smooth muscle cell migration and proliferation, expansion of extracellular matrix, neo-angiogenesis, tissue necrosis, and mineralization at later stages. The ultimate characteristics of an atherosclerosis plaque at any given time depend on the relative contribution of each of these features.

Coronary angiography Coronary angiography is a procedure that uses X-ray imaging and depicts arteries as a planar silhouette of the contrast-filled lumen. Angiographic disease assessment is based on the comparison of the stenotic segment with the adjacent, "normal appearing" coronary. It does not provide visualization of the vessel wall and is not suitable for assessment of atherosclerosis. Moreover, angiography interpretation is flawed by large inter- and intra-observer variability and usually underestimates the severity of the disease and vessel dimensions.

Intravascular ultrasound (IVUS) It is a three-dimensional imaging modality which provides a complete assessment of the coronary vessel wall. The IVUS image is the result of reflected ultrasound waves that are converted to electrical signals and sent to an external processing system for amplification, filtering, and scan-conversion. Its axial resolution is approximately 100 μm, while lateral resolution reaches 200–250 μm in conventional IVUS system (20–40 MHz).

IVUS-based imaging modalities IVUS-based imaging modalities are virtual histology, iMAP, integrated backscattered IVUS, and echogenicity. IVUS gray scale uses only the amplitude of the signal, while most of the IVUS-based imaging modalities use the radiofrequency data that lies underneath the amplitude.

Lipid core plaque (LCP) Lipid core plaque of interest is defined as a lipid core >60° in circumferential extent, >200-μm thick, with a mean fibrous cap thickness <450 μm.

Near-infrared spectroscopy catheter system (NIRS) NIRS is an imaging modality that uses near-infrared light to detect lipid. Since NIRS is coupled with an IVUS probe, the geometry of the plaques can be assessed simultaneously. It does not provide information about inflammation nor about other tissue types apart from lipid. Indeed, this NIRS catheter allows to analyze lipid core plaque "in vivo" because it can penetrate the blood and several millimeters into the tissue.

Necrotic core From the histological point of view, necrotic core can be defined as an area in which the extracellular matrix is lacking (total loss of collagen by picrosirius red staining) and replaced by dead cells and cellular debris (fragmented nuclei by hematoxylin and eosin staining). It is known to be the most thrombogenic component of atheromatous plaques, largely due to its high content in tissue factor, which sets off the exogenous coagulation cascade and is a major determinant in the equilibrium between pro- and anticoagulant processes.

Optical coherence tomography (OCT) OCT is a light-based imaging modality that can be applied in vivo in coronary arteries. By using reflected light instead of sound, OCT is able to provide images with a level of resolution (range 10–40 μm) tenfold higher than conventional IVUS. OCT can offer very valuable structural and compositional information about plaques causing coronary stenosis. It can accurately identify features related with culprit plaques in acute coronary syndromes such as plaque rupture and subsequent thrombosis. Furthermore, its ability to measure the fibrous cap and to detect macrophages makes of OCT one of the most promising techniques for the detection of plaques at high risk of rupture.

Thin fibrous cap atheroma (TCFA) A thin, fibrous cap (<65 μm) infiltrated by macrophages and lymphocytes with rare or absence of smooth muscle cells and a relatively large underlying necrotic core; intraplaque hemorrhage/fibrin may be present.

Virtual histology (VH-IVUS) Virtual histology is a spectral analysis of radiofrequency ultrasound signals using radiofrequency data. It provides information on four tissue types: fibrous, fibrofatty, necrotic core, and dense calcium. Evaluation of the layout of these four different tissue types gives information on different coronary plaque types. As virtual histology is an IVUS-derived technique, its axial resolution is limited (its axial resolution is approximately 100 μm, while lateral resolution reaches 250 μm). This precludes assessment of thin fibrous cap. Moreover, virtual histology does not provide information on thrombus and inflammation.

Introduction

The In Vivo Assessment of Atheroma Plaque

Atherosclerotic process is characterized by an intricate sequence of events that involve: extracellular lipid accumulation, endothelial dysfunction, leukocyte recruitment, intracellular lipid accumulation (foam cells), smooth muscle cell migration and proliferation, expansion of the extracellular matrix, neo-angiogenesis, tissue necrosis, and mineralization in the later stages. The ultimate characteristics of an atherosclerotic plaque at any given time depend on the relative contribution of each of these features (Virmani et al. 2000; Ross 1999). In this context, fibroatheroma with a lipid-rich necrotic core and a thin fibrous cap (TCFA) seems particularly prone to rupture and subsequently to coronary artery occlusion (Fernández-Ortiz et al. 1994). Indeed, the necrolipidic core is known as the most thrombogenic component of atheromatous plaques (Farb et al. 1996). This characteristic is mostly due to its high content in tissue factor (Thiruvikraman et al. 1996; Toschi et al. 1997), which sets off the exogenous coagulation cascade and represents a major determinant in the equilibrium between pro- and anticoagulant processes (Banner et al. 1996). TCFA is characterized by a large necrotic core containing numerous cholesterol clefts, cellular debris, and microcalcifications. In particular, the overlying fibrous cap is thin and rich in inflammatory cells, macrophages, and T lymphocytes with a few smooth muscle cells. Paralleling at the discovering of such a heterogeneous nature of the atheroma, new strategies to evaluate plaque composition and vessel architecture are emerging. Of note, coronary angiography depicts arteries as a planar silhouette of the contrast-filled lumen, therefore does not allow to assess atherosclerosis and to visualize vessel wall. Moreover, angiography interpretation is flawed by large inter- and intra-observer variability and usually underestimates the severity of the vessel disease, as well as its dimensions. Although quantitative coronary angiography has reduced the visual error, positive remodeling phenomenon makes angiography an unreliable method to assess atherosclerosis burden (Roberts and Jones 1979; Escaned et al. 1996).

In this context, grayscale intravascular ultrasound imaging (IVUS) overcomes the limitations of angiography and it is currently considered the gold standard for in vivo imaging of the wall of coronary arteries (Fujii et al. 2013; Mintz et al. 2001). In addition, it can be useful in various clinical scenarios: assessment of vessel remodeling, plaque progression/regression, ambiguous disease in vessels with aneurysmal dilatation, ostial stenoses, disease located at branching points or in the left main, tortuous or calcified segments, eccentric disease, complex disease morphology, intraluminal filling defects, thrombus, dissection, and lumen dimensions after coronary intervention (Sabaté et al. 1999; Jiménez-Quevedo et al. 2006; Futamatsu et al. 2006; Jiménez-Quevedo et al. 2005; Kay et al. 2000b).

The IVUS image is the result of reflected ultrasound waves that are converted to electrical signals and sent to an external processing system for amplification,

filtering, and scan-conversion. After placing the transducer, the beam remains almost parallel for a short distance ("near field"; better image quality) and then begins to diverge ("far field"). After encountering a transition between different materials, the beam will be partially reflected and partially transmitted, depending on tissue composition and differences in mechanical impedance between materials. Ultimately, grayscale IVUS imaging is formed by the envelope (amplitude) of the obtained radiofrequency signal.

The quality of ultrasound images is described by spatial and contrast resolution. In particular, its axial and lateral resolution reach approximately 100 and 200–250 μm in conventional IVUS system (20–40 MHz), respectively. Contrast resolution is the distribution of the gray scale of the reflected signal, and is often referred to as dynamic range.

An image of low dynamic range appears as black and white with a few levels of gray; images at high dynamic range are often softer.

However, the grayscale representation of the coronary vessel wall and plaque morphology, in combination with the limited resolution of the current IVUS catheter, makes difficult, if not impossible, to qualitatively identify the plaque morphology similarly to histopathology (Garcia-Garcia et al. 2010). For these reasons, virtual histology IVUS (VH-IVUS), an IVUS-based tissue characterization technique, has been designed to overcome these limitations. Indeed, it is able to identify the necrotic core of the coronary plaque, recently shown related to clinical risk factors and also associated with future cardiac adverse events (Nair et al. 2002, 2007; Garcia-Garcia et al. 2009a).

Tissue Characterization Using VH-IVUS

The first commercially available radiofrequency (RF) signal based tissue composition analysis tool was the so-called VH-IVUS (Volcano Therapeutics) software. It uses in-depth analysis of the backscattered RF signal in order to provide a more detailed description of the atheromatous plaque's composition. It is performed with either a 20 MHz, 2.9 F phased-array transducer catheter (Eagle EyeTM Gold, Volcano Therapeutics) or 45 MHz 3.2 F rotational catheter (Revolution, Volcano Therapeutics) that acquires ECG-gated IVUS data (Garcia-Garcia et al. 2009a). The main principle of this technique is to employ envelope amplitude of the reflected RF signals (as grayscale IVUS does) as well as underlie frequency content to analyze the tissue components present in the coronary plaque (Fig. 1). This combined information is processed using autoregressive models and thereafter in a classification tree that determines four basic plaque tissue components (Nair et al. 2007): (1) fibrous tissue (dark green), (2) fibrofatty tissue (light green), (3) necrotic core (red), and (4) dense calcium (white). The current software version assumes the presence of a media layer, artificially added and positioned just inside the outer vessel contour. This technique has been compared in several studies against histology in humans and other species (Table 1) (Nair et al. 2007; Brugaletta and Sabate 2014; Nasu et al. 2006; Granada et al. 2007; Van Herck et al. 2009; Thim et al. 2010) In

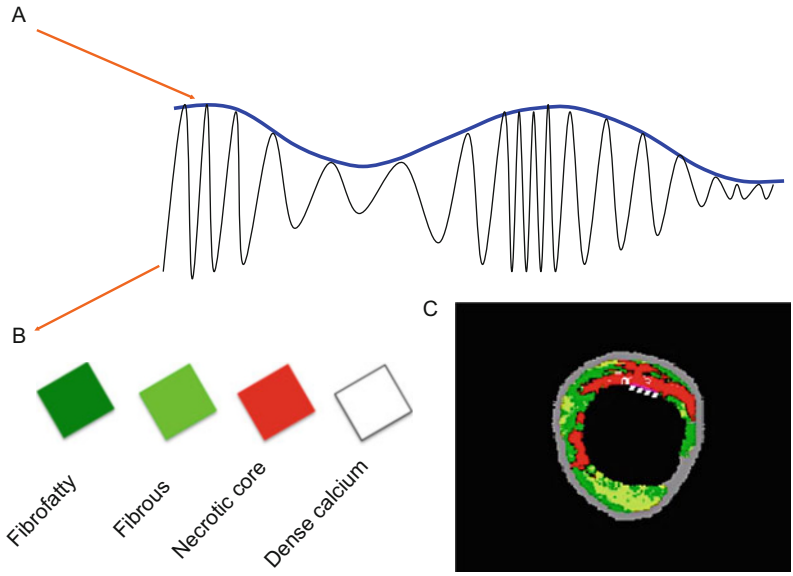

Fig. 1 Grayscale IVUS imaging is formed by the envelope (amplitude) (*A*) of the radiofrequency signal (*B*). The frequency and power of the signal commonly differ between tissues, regardless of similarities in amplitude. From the backscatter radiofrequency, virtual histology is obtained (*C*) and is able to detect four tissue types: fibrofatty, fibrous, necrotic core, and dense calcium

particular, VH-IVUS spectral analysis correlates well with histopathology, with predictive accuracy of 87.1 %, 87.1 %, 88.3 %, and 96.5 % for fibrous, fibrofatty, necrotic core, and dense calcium, respectively (Brugaletta et al. 2014; Nasu et al. 2006; Granada et al. 2007; Van Herck et al. 2009; Thim et al. 2010).

VH-IVUS Diagnostic Application

Plaque Characterization

VH-IVUS (Fig. 2) is able to define the various phases of atherosclerosis (Garcia-Garcia et al. 2006). More specifically, the definition of an "IVUS-derived TCFA" consists in a lesion fulfilling the following criteria in at least three consecutive frames: (1) plaque burden >40 %, and (2) confluent necrotic core >10 % in direct contact with the lumen (i.e., no visible overlying tissue) (Garcia-Garcia et al. 2006). Using this refined definition of "IVUS derived TCFA," in patients with acute coronary syndrome (ACS) who underwent IVUS of all three epicardial coronaries, there were "2 IVUS-derived TCFA" per patient, with half of them showing outward remodeling. Accordingly, Hong et al. (2008) described the frequency and distribution of TCFA in a 3-vessel VH-IVUS study of patients with ACS ($n = 105$) or stable angina (SA; $n = 107$). There were 2.5 ± 1.5 TCFAs per patient in the ACS group

Table 1 Comparison of VH-IVUS with histology in humans and other species

Author	Type of study	Year	Principal results
Nair et al.	Ex vivo	2002	Coronary plaque classification with IVUS RF data analysis: Autoregressive classification schemes performed better than those from classic Fourier spectra with accuracies of 90.4 % for FT, 92.8 % for fibrolipidic, 90.9 % for calcified, and 89.5 % for calcified-necrotic regions in the training data set and 79.7 %, 81.2 %, 92.8 %, and 85.5 %, respectively, in the test data
Nasu et al.	In vivo	2006	Accuracy of in vivo coronary plaque morphology assessment: a validation study of in vivo VH compared with in vitro histopathology. Predictive accuracy from all patients data: 87.1 % for FT, 87.1 % for FF, 88.3 % for NC, and 96.5 % for DC regions, respectively. Sensitivities: NC 67.3 %, FT 86 %, FF 79.3 %, DC 50 %. Specificities: NC 92.9 %, FT 90.5 %, FF 100 %, DC 99 %
Nair et al.	Ex vivo	2007	Automated coronary plaque characterization with IVUS backscatter: ex vivo validation. Overall predictive accuracies were 93.5 % for FT, 94.1 % for FF, 95.8 % for NC, and 96.7 % for DC. Sensitivities: NC 91.7 %, FT 95.7 %, FF 72.3 %, DC 86.5 %. Specificities: NC 96.6 %, FT 90.9 %, FF 97.9 %, DC 98.9 %
Granada et al.	In vivo	2007	In vivo plaque characterization using VH-IVUS in a porcine model of complex coronary lesions: compared with histology, VH-IVUS correctly identified the presence of FT, FF, and necrotic tissue in 58.33 %, 38.33 %, and 38.33 % of lesions, respectively. Sensitivities: FT 76.1 %, FF 46 %, and NC 41.1 %
Van Herk et al.	In vivo	2009	Validation of in vivo plaque characterization by VH in a rabbit model of atherosclerosis: VH-IVUS had a high sensitivity, specificity, and positive predictive value for the detection of noncalcified TCFA (88 %, 96 %, 87 %, respectively) and calcified TCFA (95 %, 99 %, 93 %, respectively). These values were respectively 82 %, 94 %, 85 % for noncalcified FA and 78 %, 98 %, 84 % for calcified FA. The lowest values were obtained for pathologic intimal thickening (74 %, 92 %, 70 %, respectively). For all plaque types, VH-IVUS had a kappa-value of 0.79
Thim et al.	Ex vivo	2010	Unreliable assessment of NC by VHTM IVUS in porcine coronary artery disease: no correlations were found between the size of the NC determined by VH-IVUS and histology. VH-IVUS displayed NCs in lesions lacking cores by histology
Brugaletta et al.	In vivo	2014	Qualitative and quantitative accuracy of VH-IVUS for detection of NC in human coronary arteries: VH had high sensitivity, but low specificity and low positive predictive value for NC identified by histology. In addition, it was not able to accurately quantify its size in the histological specimen

DC dense calcium, *FA* fibroatheroma, *FF* fibrofatty, *FT* fibrous tissue, *IVUS* intravascular ultrasound, *NC* necrotic core, *RF* radiofrequency, *TFCA* thin fibrous cap atheroma, *VH* virtual histology

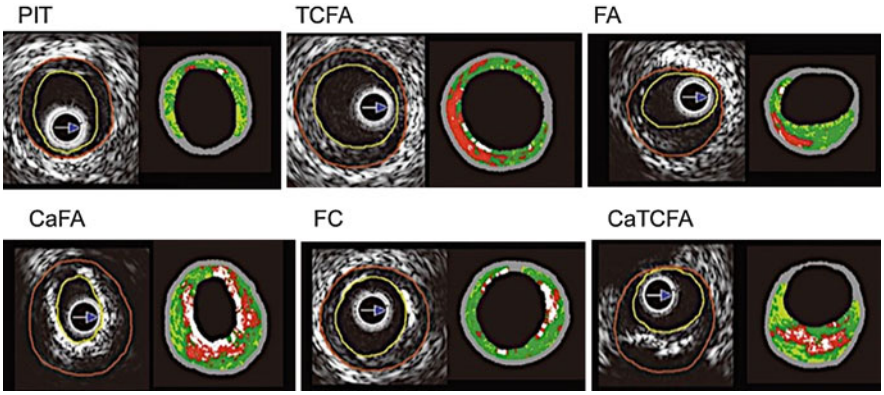

Fig. 2 Examples of various atherosclerotic plaques in different stages, classified by virtual histology (VH). Lumen contour (*yellow line*) and vessel contour (*red line*) are shown. In the VH images, necrotic core is coded as *red*, dense calcium as *white*, fibrous tissue as *dark green*, and fibrofatty tissue as *light green. CaFA* calcified fibroatheroma, *CaTCFA* calcified thin-cap fibroatheroma, *FA* fibroatheroma, *FC* fibrocalcific plaque, *PIT* pathological intimal thickening, *TCFA* thin-cap fibroatheroma

and 1.7 ± 1.1 in the SA group, respectively ($P < 0.001$). Presentation of ACS was the only independent predictor for multiple VH-derived TCFA (VH-TCFA) ($P = 0.011$), and 83 % of VH-TCFAs were located within the first 40 mm of the coronary artery. By use of VH-IVUS, the serial changes in VH plaque type have been also investigated. In particular, Kubo et al. (2010) showed that most VH-TCFAs healed during a 12-month follow-up. However, along the follow-up period, new VH-TCFA developed and pathologic intimal thickening and necrotic core plaques had a significant progression compared with fibrotic and fibrocalcific plaques in terms of increase in plaque area and decrease in lumen. Moreover, a recent study using VH demonstrated that, in patients with ST elevation myocardial infarction after thrombolysis, the necrotic core content of culprit plaques is strongly associated with the degree of flow restoration. Indeed, there were significant differences in the relative necrotic core content, both in proportion to the whole plaque volume (26.3 % vs. 29.9 %; $p = 0.016$), as well as in area fraction at the largest necrotic core site (31.5 % vs. 40.3 %; $p < 0.001$) between patients with TIMI 3 versus those with TIMI 1–2 flow grade (Giannopoulos et al. 2014).

The potential value of VH-TCFA in the prediction of adverse coronary events was evaluated in an international multicenter prospective study, the Providing Regional Observations to Study Predictors of Events in the Coronary Tree study (PROSPECT study) (Stone et al. 2011).

The PROSPECT trial was conducted in ACS patients, all of whom underwent percutaneous coronary intervention (PCI) for their culprit lesion at baseline followed by angiography and VH-IVUS of the three major coronary arteries. A TCFA with a minimum luminal area ≤ 4 μm^2 and a large plaque burden ≥ 70 % had a 17.2 % likelihood of causing an event within 3 years. Interestingly, the anticipated high

frequency of acute thrombotic cardiovascular events did not occur, with only a 1 % rate of myocardial infarction (MI) and no deaths directly attributable to nonculprit vessels over the 3 years of follow-up. These results suggest that nonculprit yet obstructive coronary plaques were most likely to be associated with increasing symptoms rather than thrombotic acute events, with 8.5 % of patients presenting with worsening angina and 3.3 % with unstable angina. Of note, the findings of the PROSPECT trial were not translated in clinical practice into a percutaneous preventive treatment of VH-TCFA.

These results were recently confirmed by the VIVA study (Calvert et al. 2011). In particular, this study aimed at determining whether TCFA identified by VH-IVUS are associated with major adverse cardiac events (MACE) on individual plaque or whole patient analysis. For this purpose, 1070 with SA or troponin-positive ACS referred for PCI were prospectively enrolled and underwent 3-vessel VH-IVUS pre-PCI and also post-PCI in the culprit vessel. MACE consisted of death, MI, or unplanned revascularization. In all, 30,372 mm of VH-IVUS were analyzed. Eighteen MACE occurred in 16 patients over a median follow-up of 625 days (interquartile range, IR: 463–990 days); 1,096 plaques were classified, and 19 lesions resulted in MACE (13 nonculprit lesions and 6 culprit lesions). Nonculprit lesion factors associated with nonrestenotic MACE included VH-TCFA (hazard ratio [HR]: 7.53, $p = 0.038$) and plaque burden >70 % (HR: 8.13, $p = 0.011$). VH-TCFA (HR: 8.16, $p = 0.007$), plaque burden >70 % (HR: 7.48, $p = 0.001$), and minimum luminal area <4 μm^2 (HR: 2.91, $p = 0.036$) were associated with total MACE. On patient-based analysis, the only factor associated with nonrestenotic MACE was 3-vessel noncalcified VH-TCFA (HR: 1.79, $p = 0.004$). The crucial issue of this study was represented by the association between VH-IVUS–based plaque classification and total and nonrestenotic MACE. In particular, nonculprit lesion plaque burden >70 % and remodeling index showed a strong correlation with nonrestenotic MACE. These results emphasize the biological importance of this association, and indicate that VH-IVUS can identify plaques at increased risk of subsequent events (Calvert et al. 2011).

VH-IVUS Research Application

Assessment of Drug Effect on Atherosclerosis Progression/Regression

VH-IVUS has so far been used in various studies to show serial changes of plaque composition in patients treated with various drugs (Table 2). In particular, Nasu et al. (2009) demonstrated that treatment with fluvastatin for 1 year in patients with SA ($n = 80$) caused a significant regression of the plaque volume and caused changes in the atherosclerotic plaque composition with a significant reduction of the fibrofatty volume ($P < 0.0001$). This change in fibrofatty volume had a significant correlation with changes in the low-density lipoprotein/cholesterol (LDL) level ($r = 0.703$, $P < 0.0001$) and in the high-sensitivity C-reactive protein level ($r = 0.357$, $P = 0.006$) (Nasu et al. 2009; Kovarnik et al. 2012). Of note, the

Table 2 Serial changes of plaque composition by VH-IVUS in patients treated with various statins

Author	Type	Year	Treatment	Patients	Period	Parameter	Results
Serruyus et al.	RCT	2008	Darapladib placebo	175 155	12 months	NC volume by VH-IVUS	Darapladib reduced NC
Nasu et al.	Obs	2009	Fluvastatin Control	40 40	12 months	Overall tissue characterization by VH-IVUS	Fluvastatin reduced plaque and FF volume
Hong et al.	RCT	2009	Simvastatin Rosuvastatin	50 50	12 months	Overall tissue characterization by VH-IVUS	Both reduced NC and increased FF volume
Toi et al.	RCT	2009	Atorvastatin Pitavastatin	80 80	2–3 week	Overall tissue characterization by VH-IVUS	Pitavastatin reduced plaque and FF volumes
Räber et al. (2015)	Obs	2014	Rosuvastatin	103	13 months	Overall tissue characterization by IVUS and RF-IVUS	Rosuvastatin reduced coronary atherosclerosis without change in RF-IVUS defined NC or plaque phenotype

FF fibrofatty, *NC* necrotic core, *OBS* observational, *RCT* randomized controlled trial, *RF* radiofrequency, *VH-IVUS* virtual histology intravascular ultrasound

necrotic core did not change significantly. The same data were found with the use of pitavastatin (Toi et al. 2009). In another study, Hong et al. (2009) randomized 100 patients with SA and ACS to either rosuvastatin 10 mg or simvastatin 20 mg for 1 year, showing a significant decrease of overall necrotic core volume ($P = 0.010$) and an increase of fibrofatty plaque volume ($P = 0.006$) after statin treatment. In particular, there was a decrease in the necrotic core volume ($P = 0.015$) in the rosuvastatin-treated subgroup. Results from multiple stepwise logistic regression analysis identified the baseline high-density lipoprotein/cholesterol level as the only independent clinical predictor of decrease in the necrotic core volume ($P = 0.040$, odds ratio 1.044, 95 % confidence interval 1.002–1.089).

Again, the IBIS-2 study (Serruys et al. 2008) compared the effects of 12 months of treatment with darapladib (oral Lp-PLA2 inhibitor, 160 mg daily) versus placebo in 330 stable and no-stable patients. In placebo group, necrotic core volume increased significantly, whereas darapladib halted this increase, resulting in a significant treatment difference of -5.2 mm^3 ($P = 0.012$). Remarkably, these intraplaque compositional changes occurred without a significant treatment difference in total atheroma volume. However, despite all these data, a direct association between a decrease in plaque size and/or plaque composition and a reduction in clinical events has not yet been described. Indeed, the latest studies revealed that darapladib did not decrease the risk of MACE both in patients with ACS (O'Donoghue et al. 2014) and with stable coronary artery disease (White et al. 2014). The best attempt using serial IVUS was a pooled analysis of 4,137 patients from six clinical trials (Nicholls et al. 2010); percent atheroma volume (PAV) increased by 0.3 % ($p < 0.001$) and 19.9 % of subjects experienced MACE (0.9 % death, 1.8 % MI, 18.9 % coronary revascularization). Greater baseline PAVs were observed in patients who experienced MI (42.2 +/− 9.6 % vs. 38.6 +/− 9.1 %, $p = 0.001$), coronary revascularization (41.2 +/− 9.3 % vs. 38.1 +/− 9.0 %, $p < 0.001$), or MACE (41.3 +/− 9.2 % vs. 38.0 +/− 9.0 %, $p < 0.001$). Each standard deviation increase in PAV was associated with a 1.32-fold (95 % confidence interval, CI: 1.22–1.42; $p < 0.001$) greater likelihood of experiencing a MACE. During follow-up (21.1 +/− 3.7 months), PAV but not total atheroma volume was greatly increased in subjects who experienced MACE compared with those who did not (0.95 +/− 0.19 % vs. 0.46 +/− 0.16 %, $p < 0.001$). Each standard deviation increase in PAV was associated with a 1.20-fold (95 % confidence interval: 1.10–1.31; $p < 0.001$) greater risk for MACE. Multivariate analysis revealed that factors associated with MACE included baseline PAV ($p < 0.0001$), change in PAV ($p = 0.002$), smoking ($p = 0.0002$), and hypertension ($p = 0.01$).

Recently, the IBIS4 aimed at quantifying the impact of high-intensity statin therapy (40 mg, day through 13 months) on plaque burden, composition, and phenotype in non–infarct-related arteries of 103 STEMI patients undergoing primary PCI, using IVUS and RF IVUS. After 13 months, low-density lipoprotein cholesterol decreased from a median of 3.29 to 1.89 mmol/L ($P < 0.001$), whereas high-density lipoprotein cholesterol levels increased from 1.10 to 1.20 mmol/L ($P < 0.001$). PAV of the non–infarct-related arteries decreased by -0.9 % (95 % CI: -1.56 to -0.25, $P = 0.007$). However, percent necrotic core remained

unchanged (−0.05 %, 95 % CI: −1.05 to 0.96 %, $P = 0.93$) as did the number of RF-IVUS defined TCFA (124 vs. 116, $P = 0.15$) (Räber et al. 2015).

Vascular Response to Endovascular Device

IVUS has been extensively used as surrogate endpoint in stent trials, primarily to assess effectiveness of devices as it relates to neo-intimal proliferation. IVUS was an essential investigational tool during initial clinical testing of drug eluting stent (DES) (Jiménez-Quevedo et al. 2006; Kay et al. 2000a), confirming the dramatic suppression of neo-intimal proliferation, revealing new patterns of restenosis and establishing intravascular imaging metrics of stent optimization.

Recently, the feasibility and safety of a bioabsorbable stent everolimus-eluting stent (BVS) was also assessed with intravascular imaging. In this context, a prospective open-label study, enrolling 30 patients with a single de novo lesion treated with BVS, showed IVUS-VH changes with reduction of RF backscattering by polymeric struts (Garcia-Garcia et al. 2009b) at 6 months follow-up. Again, another study by Brugaletta et al. (2011a) examined the temporal IVUS-VH changes in composition of the plaque behind the struts following BVS implantation, at 6 month follow-up. Compared to baseline, there was an increase in both the area of plaque behind the struts ($P = 0.005$) and the external elastic membrane area ($P = 0.006$). Furthermore, they showed a significant progression in the "necrotic core" ($P = 0.010$) and fibrous tissue area ($P = 0.027$). Hence, serial IVUS-VH analysis of BVS-treated lesions at 6 months follow-up demonstrated a progression in the necrotic core and fibrous tissue content of plaque behind the struts.

Combined Used of Multiple Image Technologies

VH-IVUS OCT Applications

In the future, integration of multiple image technologies in a single catheter is likely to provide a more comprehensive assessment of the coronary vasculature. In particular, the combined use of IVUS-VH analysis and optical coherence tomography (OCT) seems to improve the accuracy for TCFA assessment and the quantification of necrotic core (Gonzalo et al. 2009; Sawada et al. 2008). This represents a crucial point, considering that the detection of plaques with high risk of rupture could prevent future occurrence of ACS. On the one hand, if RF data analysis by VH-IVUS allows to classify the atherosclerotic plaques (fibrous, fibrofatty, dense calcium, and necrotic core) and quantify the necrotic core (Nair et al. 2007; Brugaletta et al. 2014), it cannot visualize the thin fibrous cap because of its limited resolution (>100 μm) (Sawada et al. 2008). Conversely OCT can provide a high-resolution image (10–20 μm) of the thin fibrous cap, but it is not able to detected a large and deep lipid core because of its limited penetration (<2 mm) (Matsumoto et al. 2007; Jang et al. 2002; Yabushita et al. 2002).

Sawada et al. (2008) delucidated the feasibility of the combined use of VH-IVUS and OCT to detect in vivo TCFA and to clarify the lesion characteristics of TCFA.

They identified, in 56 patients with angina, 126 plaques using both VH-IVUS and OCT. In particular, "IVUS-derived TCFA" was defined as an abundant necrotic core (>10 % of the cross-sectional area) in contact with the lumen (NCCL) and percentage plaque-volume >40 %, whereas "OCT-derived TCFA" was defined as a fibrous cap thickness of <65 μm overlying a low-intensity area with an unclear border. Plaque meeting both TCFA criteria was identified as "definite-TCFA." Sixty-one plaques were diagnosed as "IVUS-derived TCFA" and 36 plaques as "OCT-derived TCFA." Twenty-eight plaques were diagnosed as "definite-TCFA"; the remaining 33 "IVUS-derived TCFA" had a non-thin-cap and 8 "OCT-derived TCFA" had a non-NCCL. These lesions were characterized by a larger reference diameter, minimum lumen diameter, and minimum vessel volume ($p = 0.002$, $p = 0.004$, $p = 0.01$, respectively), as well as severely calcified components compared with "definite-TCFA" ($p = 0.01$). When a target vessel or plaque is large, the optical signal might be attenuated by the plaque and failed to identify plaque morphology. Furthermore, it might also be sometimes difficult to discriminate between lipid and calcified lesions because both these appear as low-intensity images, usually differentiated in OCT by an unclear border (lipid) or a clear border (calcium). In this regard, large calcified lesions are likely to be misdiagnosed as TCFA by OCT examination. Ultimately, the positive ratio of VH-IVUS for detecting definite-TCFA was 45.9 % and that for OCT 77.8 %. Hence, the use of complementary tools such as VH-IVUS and OCT might be a feasible approach for more accurate detection of TCFA.

NIRS-VH-IVUS Applications

A near-infrared spectroscopy (NIRS) catheter system (Lipiscan; InfraReDx Inc) has been recently developed for invasive detection of the lipid core in plaque (LCP) composition "in vivo" (Gardner et al. 2008; Waxman et al. 2009; Brugaletta et al. 2011b), penetrating the blood and several millimeters into the tissue. Moreover, it overcomes the problem of cardiac motion because it uses an ultrafast scanning laser and provides a chemical measure of the LCP target of interest (Garcia-Garcia et al. 2010; Moreno et al. 2002). In the last years, identification of LCP with NIRS has been showed to improve the safety of stenting, optimize the length of vessel to stent, ensure an adequate stent implantation, and also detect the lipid-core lesions at higher risk of distal embolization, possibly leading to effective use of distal embolic protection devices in the native coronaries (Oemrawsingh et al. 2003; Sakhuja et al. 2010; Waxman et al. 2010). Recently, a "head to head" comparison between VH-IVUS and NIRS for the identification of LCP/necrotic core rich plaques has been performed (Fig. 3). Larger coronary plaques, identified by grayscale IVUS, were more likely to be recognized as LCP and as necrotic-core rich plaques by NIRS and VH, respectively. However, the correlation between NIRS and VH was poor (Brugaletta et al. 2011b; Brugaletta and Sabaté 2014). Of note, for the validation of NIRS, LCP was defined as a fibroatheroma with lipid core >60° in circumferential extent, >200 μm thick, with a fibrous cap having a mean thickness <450 μm and correlated with each chemogram block (Gardner et al. 2008). On the contrary, for the

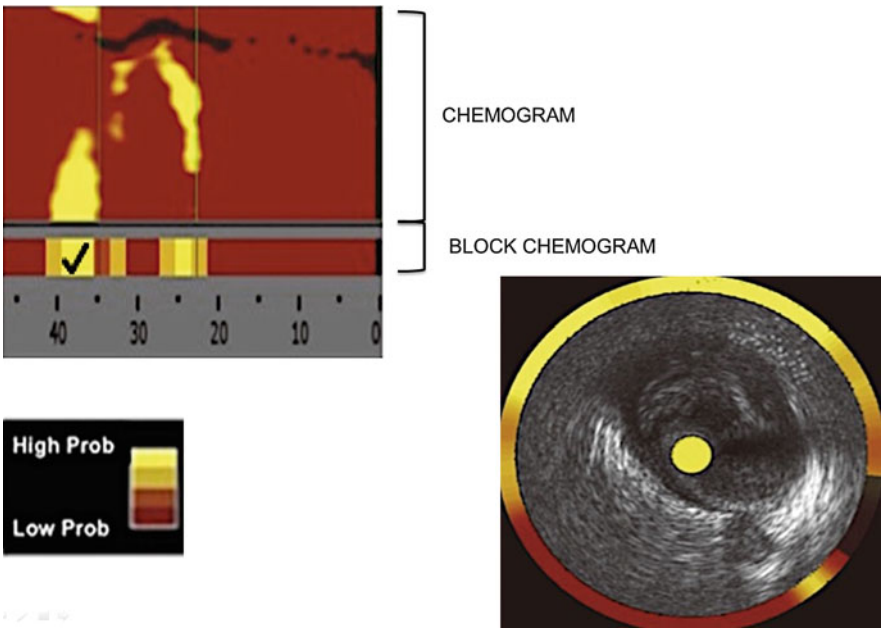

Fig. 3 At the *top left*, image obtained by NIRS displayed as a chemogram and block chemogram. The chemogram shows the scanned arterial segment as a map, whereas the block chemogram shows the presence of lipid core as a 2-mm segment using the top 90th percentile information within each 2-mm segment. The probability of lipid is displayed in a color scale from *red* (low probability) to *yellow* (high probability), through *orange* and *tan*. At the *bottom right*, acquisition with a combined NIRS-IVUS catheter. Surrounding the IVUS image, the colors define the presence of lipid (*red* = low probability/*yellow* = high probability). Note an IVUS plaque from 11 to 2 o'clock, coded as lipid-core rich by NIRS. *IVUS* intravascular ultrasound, *NIRS* near-infrared spectroscopy

validation of VH-IVUS, necrotic core was defined as the region comprising cholesterol clefts and foam cells. Some lipid components in the presence of collagen are also considered as fibrofatty tissue (Nair et al. 2002). Moreover, it should be taken in account that if VH is based on pattern classification of backscattering ultrasound signal, NIRS is based on near-infrared spectral signals. Ultimately, NIRS-IVUS device might be employed in the identification of vulnerable plaque (Brugaletta et al. 2012; Madder et al. 2013), and in the development of anti-atherosclerotic medications by providing a surrogate endpoint in plaque regression/stabilization studies (Simsek et al. 2012).

Conclusions

VH-IVUS has been shown to identify coronary plaque morphology similarly to histopathology. In particular, it is able to identify the necrotic core content that has been variously related to clinical risk factors, and also associated with the development of cardiac adverse events. In the next years, an extensive use of VH-IVUS,

alone or combined with other image technologies (e.g., OCT and NIRS), might improve the accuracy of TCFA assessment and the quantification of necrotic core.

Potential Applications to Prognosis, Other Diseases, or Conditions

The potential value of VH-TCFA in the prediction of adverse coronary events was evaluated in two recent studies: PROSPECT and VIVA trials.

In particular, the PROSPECT study showed that a TCFA with a minimum luminal area $\leq 4\ \mu m^2$ and a large plaque burden $\geq 70\ \%$ had a 17.2 % likelihood of causing an event within 3 years; the anticipated high frequency of acute thrombotic cardiovascular events did not occur, with only a 1 % rate MI and no deaths directly attributable to nonculprit vessels over the 3 years of follow-up. These results suggest that nonculprit, yet obstructive coronary plaques, were most likely to be associated with increasing symptoms rather than thrombotic acute events, with 8.5 % of patients presenting with worsening angina and 3.3 % with unstable angina.

More recently, the VIVA trial aimed at determining whether TCFA identified by VH-IVUS are associated with MACE on individual plaque or whole patient analysis. Out of 1,096 plaques classified, 19 lesions resulted in MACE (death, MI, or unplanned revascularization): 6 culprit and 13 nonculprit lesions. Nonculprit lesion factors associated with nonrestenotic MACE included VH-TCFA (HR: 7.53, $p = 0.038$) and plaque burden >70 % (HR: 8.13, $p = 0.011$). On the other hand, VH-TCFA (HR: 8.16, $p = 0.007$), plaque burden >70 % (HR: 7.48, $p = 0.001$), and minimum luminal area $<4\ \mu m^2$ (HR: 2.91, $p = 0.036$) were associated with total MACE. On patient-based analysis, the only factor associated with nonrestenotic MACE was 3-vessel noncalcified VH-TCFA (HR: 1.79, $p = 0.004$). In conclusion, this study showed an association between VH-IVUS–based plaque classification and total and nonrestenotic MACE. In particular, nonculprit lesion plaque burden >70 % and remodeling index showed a strong correlation with nonrestenotic MACE.

Summary Points

- This chapter is focused on virtual histology, an intravascular ultrasound based tissue characterization technique that provides a classification tree that determines four basic plaque tissue components: fibrous tissue (dark green), fibrofatty tissue (light green), necrotic core (red), and dense calcium (white).
- It is currently employed in the catheterization laboratory for diagnostic purpose as plaque characterization, whereas its research applications are represented by assessment of drug effect on atherosclerosis and response to endovascular devices.
- PROSPECT and VIVA trials showed that intravascular ultrasound virtual histology is able to identify the necrotic core of the coronary plaque that has been variously related to clinical risk factors and also to the risk of adverse events.
- The combined use of intravascular ultrasound virtual histology and other image technologies (e.g., optical coherence tomography and near-infrared spectroscopy)

will be likely to provide a more comprehensive assessment of the coronary vasculature.

References

Banner DW, D'Arcy A, Chène C, et al. The crystal structure of the complex of blood coagulation factor VIIa with soluble tissue factor. Nature. 1996;380:41–6.

Brugaletta S, Sabaté M. Assessment of plaque composition by intravascular ultrasound and near-infrared spectroscopy: from PROSPECT I to PROSPECT II. Circ J. 2014;78:1531–9.

Brugaletta S, Garcia-Garcia HM, Garg S, et al. Temporal changes of coronary artery plaque located behind the struts of the everolimus eluting bioresorbable vascular scaffold. Int J Cardiovasc Imaging. 2011a;27:859–66.

Brugaletta S, Garcia-Garcia HM, Serruys PW, et al. NIRS and IVUS for characterization of atherosclerosis in patients undergoing coronary angiography. J Am Coll Cardiol Img. 2011b;4:647–55.

Brugaletta S, Garcia-Garcia HM, Serruys PW, et al. Distance of lipid core-rich plaques from the ostium by NIRS in nonculprit coronary arteries. JACC Cardiovasc Imaging. 2012;5:297–9.

Brugaletta S, Cola C, Martin-Yuste V, et al. Qualitative and quantitative accuracy of ultrasound-based virtual histology for detection of necrotic core in human coronary arteries. Int J Cardiovasc Imaging. 2014;30:469–76.

Calvert PA, Obaid DR, O'Sullivan M, et al. Association between IVUS findings and adverse outcomes in patients with coronary artery disease: the VIVA (VH- IVUS in Vulnerable Atherosclerosis) study. JACC Cardiovasc Imaging. 2011;4:894–901.

Escaned J, Baptista J, Di Mario C, et al. Significance of automated stenosis detection during quantitative angiography. Insights gained from intracoronary ultrasound imaging. Circulation. 1996;94:966–72.

Farb A, Burke AP, Tang AL, et al. Coronary plaque erosion without rupture into a lipid core. A frequent cause of coronary thrombosis in sudden coronary death. Circulation. 1996;93:1354–63.

Fernández-Ortiz A, Badimon JJ, Falk E, et al. Characterization of the relative thrombogenicity of atherosclerotic plaque components: implications for consequences of plaque rupture. J Am Coll Cardiol. 1994;23:1562–9.

Fujii K, Hao H, Ohyanagi M, et al. Intracoronary imaging for detecting vulnerable plaque. Circ J. 2013;77:588–95.

Futamatsu H, Sabaté M, Angiolillo DJ, et al. Characterization of plaque prolapse after drug-eluting stent implantation in diabetic patients: a three-dimensional volumetric intravascular ultrasound outcome study. J Am Coll Cardiol. 2006;48:1139–45.

Garcia-Garcia HM, Goedhart D, Schuurbiers JC, et al. Virtual histology and remodeling index allow in vivo identification of allegedly high risk coronary plaques in patients with acute coronary syndromes: a three vessel intravascular ultra- sound radiofrequency data analysis. EuroIntervention. 2006;2:338–44.

Garcia-Garcia HM, Mintz GS, Lerman A, et al. Tissue characterisation using intravascular radio-frequency data analysis: recommendations for acquisition, analysis, interpretation and reporting. EuroIntervention. 2009a;5:177–89.

Garcia-Garcia HM, Gonzalo N, Pawar R, et al. Assessment of the absorption process following bioabsorbable everolimus-eluting stent implantation: temporal changes in strain values and tissue composition using intravascular ultrasound radiofrequency data analysis. A substudy of the absorb clinical trial. EuroIntervention. 2009b;4:443–8.

Garcia-Garcia HM, Costa MA, Serruys PW. Imaging of coronary atherosclerosis: intravascular ultrasound. Eur Heart J. 2010;31:2456–69.

Gardner CM, Tan H, Hull EL, et al. Detection of lipid core coronary plaques in autopsy specimens with a novel catheter-based near-infrared spectroscopy system. JACC Cardiovasc Imaging. 2008;1:638–48.

Giannopoulos G, Pappas L, Synetos A, et al. Association of virtual histology characteristics of the culprit plaque with post-fibrinolysis flow restoration in ST-elevation myocardial infarction. Int J Cardiol. 2014;174:678–82.

Gonzalo N, Garcia-Garcia HM, Regar E, et al. In vivo assessment of high-risk coronary plaques at bifurcations with combined intravascular ultrasound and optical coherence tomography. JACC Cardiovasc Imaging. 2009;2:473–82.

Granada JF, Wallace-Bradley D, Win HK, et al. In vivo plaque characterization using intravascular ultra- sound: virtual histology in a porcine model of complex coronary lesions. Arterioscler Thromb Vasc Biol. 2007;27:387–93.

Hong MK, Mintz GS, Lee CW, et al. A three-vessel virtual histology intravascular ultrasound analysis of frequency and distribution of thin-cap fibroatheromas in patients with acute coronary syndrome or stable angina pectoris. Am J Cardiol. 2008;101:568–72.

Hong MK, Park DW, Lee CW, et al. Effects of statin treatments on coronary plaques assessed by volumetric virtual histology intravascular ultrasound analysis. JACC Cardiovasc Interv. 2009;2:679–88.

Jang IK, Bouma BE, Kang DH, et al. Visualization of coronary atherosclerotic plaques in patients using optical coherence tomography: comparison with intravascular ultrasound. J Am Coll Cardiol. 2002;39:604–9.

Jiménez-Quevedo P, Sabaté M, Angiolillo D, et al. LDL-cholesterol predicts negative coronary artery remodelling in diabetic patients: an intravascular ultrasound study. Eur Heart J. 2005;26:2307–12.

Jiménez-Quevedo P, Sabaté M, Angiolillo DJ, et al; DIABETES Investigators. Vascular effects of sirolimus-eluting versus bare-metal stents in diabetic patients: three-dimensional ultrasound results of the Diabetes and Sirolimus-Eluting Stent (DIABETES) Trial. J Am Coll Cardiol. 2006;47:2172–9.

Kay IP, Sabate M, Van Langenhove G, Costa MA, et al. Outcome from balloon induced coronary artery dissection after intracoronary beta radiation. Heart. 2000a;83:332–7.

Kay IP, Sabaté M, Costa MA, et al. Positive geometric vascular remodeling is seen after catheter-based radiation followed by conventional stent implantation but not after radioactive stent implantation. Circulation. 2000b;102:1434–9.

Kovarnik T, Mintz GS, Skalicka H, et al. Virtual histology evaluation of atherosclerosis regression during atorvastatin and ezetimibe administration: HEAVEN study. Circ J. 2012;76:176–83.

Kubo T, Maehara A, Mintz GS, et al. The dynamic nature of coronary artery lesion morphology assessed by serial virtual histology intravascular ultrasound tissue characterization. J Am Coll Cardiol. 2010;55:1590–7.

Madder RD, Goldstein JA, Madden SP, et al. Detection by near-infrared spectroscopy of large lipid core plaques at culprit sites in patients with acute ST-segment elevation myocardial infarction. JACC Cardiovasc Interv. 2013;6:838–46.

Matsumoto D, Shite J, Shinke T, et al. Neointimal coverage of sirolimus-eluting stents at 6-month follow-up: evaluated by optical coherence tomography. Eur Heart J. 2007;28:961–7.

Mintz GS, Nissen SE, Anderson WD, et al. American College of Cardiology Clinical Expert Consensus Document on Standards for Acquisition, Measurement and Reporting of Intravascular Ultrasound Studies (IVUS): a report of the American College of Cardiology Task Force on Clinical Expert Consensus Documents. J Am Coll Cardiol. 2001;37:1478–92.

Moreno PR, Lodder RA, Purushothaman KR, et al. Detection of lipid pool, thin fibrous cap, and inflammatory cells in human aortic atherosclerotic plaques by near-infrared spectroscopy. Circulation. 2002;105:923–7.

Nair A, Kuban BD, Tuzcu EM, Schoenhagen P, et al. Coronary plaque classification with intravascular ultrasound radiofrequency data analysis. Circulation. 2002;106:2200–6.

Nair A, Margolis MP, Kuban BD, et al. Automated coronary plaque characterisation with intravascular ultrasound backscatter: ex vivo validation. EuroIntervention. 2007;3:113–20.

Nasu K, Tsuchikane E, Katoh O, et al. Accuracy of in vivo coronary plaque morphology assessment: a validation study of in vivo virtual histology compared with in vitro histopathology. J Am Coll Cardiol. 2006;47:2405–12.

Nasu K, Tsuchikane E, Katoh O, et al. Effect of fluvastatin on progression of coronary atherosclerotic plaque evaluated by virtual histology intravascular ultrasound. JACC Cardiovasc Interv. 2009;2:689–96.

Nicholls SJ, Hsu A, Wolski K, Hu B, et al. Intravascular ultrasound-derived measures of coronary atherosclerotic plaque burden and clinical outcome. J Am Coll Cardiol. 2010;55:2399–407.

O'Donoghue ML, Braunwald E, White HD, et al. Effect of darapladib on major coronary events after an acute coronary syndrome: the SOLID-TIMI 52 randomized clinical trial. JAMA. 2014;312:1006–15.

Oemrawsingh PV, Mintz GS, Schalij MJ, et al. Intravascular ultrasound guidance improves angiographic and clinical outcome of stent implantation for long coronary artery stenoses: final results of a randomized comparison with angiographic guidance (TULIP Study). Circulation. 2003;107:62–7.

Räber L, Taniwaki M, Zaugg S, Kelbæk H, Roffi M, Holmvang L, Noble S, Pedrazzini G, Moschovitis A, Lüscher TF, Matter CM, Serruys PW, Jüni P, Garcia-Garcia HM, Windecker S; IBIS 4 (Integrated Biomarkers and Imaging Study-4) Trial Investigators. Effect of high-intensity statin therapy on atherosclerosis in non-infarct-related coronary arteries (IBIS-4): a serial intravascular ultrasonography study. Eur Heart J. 2015;36:490–500.

Roberts WC, Jones AA. Quantitation of coronary arterial narrowing at necropsy in sudden coronary death: analysis of 31 patients and comparison with 25 control subjects. Am J Cardiol. 1979;44:39–45.

Ross R. Atherosclerosis: an inflammatory disease. N Engl J Med. 1999;340:115–26.

Sabaté M, Kay IP, de Feyter PJ, et al. Remodeling of atherosclerotic coronary arteries varies in relation to location and composition of plaque. Am J Cardiol. 1999;84:135–40.

Sakhuja R, Suh WM, Jaffer FA, et al. Residual thrombogenic substrate after rupture of a lipid-rich plaque: possible mechanism of acute stent thrombosis? Circulation. 2010;122:2349–50.

Sawada T, Shite J, Garcia-Garcia HM, et al. Feasibility of combined use of intravascular ultrasound radiofrequency data analysis and optical coherence tomography for detecting thin-cap fibroatheroma. Eur Heart J. 2008;29:1136–46.

Serruys PW, Garcia-Garcia HM, Buszman P, et al. Effects of the direct lipoprotein-associated phospholipase A(2) inhibitor darapladib on human coronary atherosclerotic plaque. Circulation. 2008;118:1172–82.

Simsek C, Garcia-Garcia HM, van Geuns RJ, et al. The ability of high dose rosuvastatin to improve plaque composition in non-intervened coronary arteries: rationale and design of the Integrated Biomarker and Imaging Study-3 (IBIS-3). EuroIntervention. 2012;8:235–41.

STABILITY Investigators, White HD, Held C, Stewart R, et al. Darapladib for preventing ischemic events in stable coronary heart disease. N Engl J Med. 2014;370:1702–11.

Stone GW, Maehara A, Lansky AJ, et al; PROSPECT Investigators. A prospective natural-history study of coronary atherosclerosis. N Engl J Med. 2011;364:226–35.

Thim T, Hagensen MK, Wallace-Bradley D, et al. Unreliable assessment of necrotic core by virtual histology intravascular ultrasound in porcine coronary artery disease. Circ Cardiovasc Imaging. 2010;3:384–91.

Thiruvikraman SV, Guha A, Roboz J, et al. In situ localization of tissue factor in human atherosclerotic plaques by binding of digoxigenin-labeled factors VIIa and X. Lab Invest. 1996;75:451–61.

Toi T, Taguchi I, Yoneda S, Kageyama M, et al. Early effect of lipid-lowering therapy with pitavastatin on regression of coronary atherosclerotic plaque: comparison with atorvastatin. Circ J. 2009;73:1466–72.

Toschi V, Gallo R, Lettino M, et al. Tissue factor modulates the thrombogenicity of human atherosclerotic plaques. Circulation. 1997;95:594–9.

Van Herck J, De Meyer G, Ennekens G, et al. Validation of in vivo plaque characterisation by virtual histology in a rabbit model of atherosclerosis. EuroIntervention. 2009;5:149–56.

Virmani R, Kolodgie FD, Burke AP, et al. Lessons from sudden coronary death: a comprehensive morphological classification scheme for atherosclerotic lesions. Arterioscler Thromb Vasc Biol. 2000;20:1262–75.

Waxman S, Dixon SR, L'Allier P, et al. In vivo validation of a catheter-based near-infrared spectroscopy system for detection of lipid core coronary plaques: initial results of the SPECTACL study. JACC Cardiovasc Imaging. 2009;2:858–68.

Waxman S, Freilich MI, Suter MJ, et al. A case of lipid core plaque progression and rupture at the edge of a coronary stent: elucidating the mechanisms of drug-eluting stent failure. Circ Cardiovasc Interv. 2010;3:193–6.

Yabushita H, Bouma BE, Houser SL, et al. Characterization of human atherosclerosis by optical coherence tomography. Circulation. 2002;106:1640–5.